Journal of Spacecraft and Rockets

VOLUME 1 SEPTEMBER-OCTOBER 1964 NUMBER 5

Recent Developments in Wind-Tunnel Testing Techniques at Transonic and Supersonic Speeds

RUDOLPH W. HENSEL
ARO, Inc., Arnold Air Force Station, Tenn.

Introduction

TRANSONIC and supersonic wind tunnels have in recent years become quite diversified tools because of the variety of new problems that have arisen in the development of ballistic missile, orbital, and space systems. In many cases, these new problem areas and requirements have made it necessary to evolve specific wind-tunnel test techniques to assure a valid experimental investigation. The basic principles of new techniques in seven selected areas are outlined, and the merits and shortcomings are examined. In some cases there are competing techniques for the same basic purpose; these are compared critically. Conclusions are drawn concerning the limits of validity and relative accuracy, where applicable. Areas in which further technique development is needed are also outlined.

Jet Simulation

A problem of increasing concern in the design of jet-propelled vehicles is the effect of the jet exhaust on the flow over adjacent components of the vehicle. The aerodynamic aspects of this jet interference can appear as changes in stability, trim, drag, and loads, which can be either favorable or unfavorable to the vehicle performance. In subsonic aircraft, interference can be minimized by placing all surfaces outside of a predetermined influence region of the turbojet exhaust. However, at supersonic speeds, jet interaction with the external airstream produces shock waves which lead to unavoidable interference on the vehicle in many configurations. In the case of rocket engines with highly underexpanded nozzles (a common design compromise), the large jet plume that results can affect the aerodynamics near the bases of missiles.

A typical jet flow pattern from an axisymmetric supersonic nozzle at a supersonic stream velocity for values of nozzle exit to freestream static pressure ratio, p_e/p_∞, greater than approximately 3, is shown in Fig. 1. At lower pressure ratios the Mach disks are replaced by oblique shock intersections that resemble a diamond pattern. One can conclude that jet interference effects can be accurately obtained if no part of the flight vehicle is immersed in the jet, and if the exit and transmitted shock waves and the jet boundary are faithfully duplicated. For the shocks, we are concerned with both location and strength. With these conditions met, the streamlines everywhere external to the jet will be correct, and the wave disturbances from the jet will be correctly matched in location and intensity. For those cases in which jet impingement is a factor, the detailed properties within the jet to the edge of the mixing layer must be considered.

Simulation Parameters for Jet External Properties

For jet boundary matching, the first consideration is the determination of the initial jet inclination angle δ_e which is established by $\Delta\nu$, the Prandtl-Meyer expansion angle required to equalize the jet boundary pressures just downstream of the nozzle exit. Since $\Delta\nu$ is a function only of M_e, γ_e, and the ratio of p_e to the boundary pressure just

Rudolph W. Hensel is Chief of the Arnold Engineering Development Center's Propulsion Wind Tunnel Facility, a post he has held since 1956. Prior to joining ARO, Inc. in 1953, he was Chief of the Data Analysis Department at the California Institute of Technology Cooperative Wind Tunnel. While on active duty with the U. S. Army Air Force, he was Engineer-in-Charge of the 10-ft (Transonic) Wind Tunnel at Wright Field from 1944–1947. Mr. Hensel holds S.B. and S.M. degrees in aeronautical engineering from Massachusetts Institute of Technology (1942) and the Professional Degree of Aeronautical Engineer from California Institute of Technology (1944). He is an Associate Fellow Member of the AIAA.

Presented at the AIAA Aerodynamic Testing Conference, Washington, D. C., March 9–10, 1964 (no preprint number; published in bound volume of preprints of the meeting); revision received July 20, 1964. The author would like to express his appreciation to M. Pindzola, J. B. Delano, R. S. Dick, A. K. Windmueller, H. C. DuBose, T. L. Kennedy, and J. E. Robertson of the Propulsion Wind Tunnel Staff for their assistance in gathering the material presented herein and their helpful comments and suggestions, and also to Gladys Clark and Wanda Bush for their efforts in preparing the manuscript and the figures.

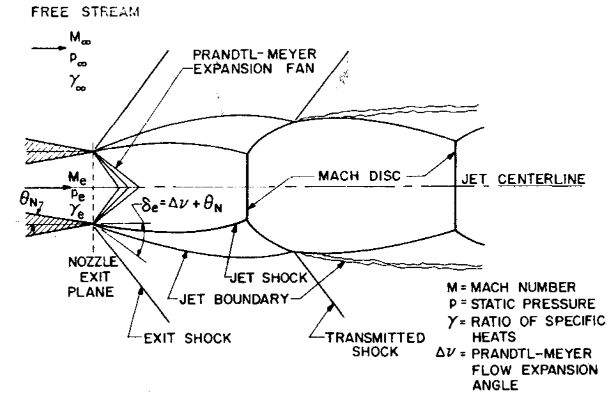

Fig. 1 Sketch of typical jet flow pattern for jet exit Mach number M_e and stream Mach number M_∞, both supersonic.

downstream of the exit, the inviscid flow streamlines near the nozzle exit are completely determined by the freestream and exit values of Mach number M_∞ and M_e, static pressure p_∞ and p_e, and ratio of specific heats γ_∞ and γ_e. It can be shown by the method of characteristics that the boundary shape variation downstream of the exit is also dependent on the same variables. Since γ_∞ and M_∞ are almost always duplicated in any specific experiment, it remains that p_e/p_∞, M_e, and γ_e must be duplicated for correct simulation; of these, p_e/p_∞ is the parameter of first-order importance in defining the jet boundary.[1-4] In most experiments, p_e and p_∞ can be controlled independently, so that duplication of p_e/p_∞ is no problem. Duplication of M_e presents no difficulty. However, γ_e matching is a problem, particularly when simulation by cold jets is desired.

Goethert and Barnes[5] have derived (by linearized theory) a simulation parameter, $\xi \equiv \gamma_e M_e^2(M_e^2 - 1)^{-1/2}$, based on the requirement that a static pressure change caused by a change in flow direction in the jet and in the external flow must be the same for the model and the full-scale vehicle. This is the same as stating that δ_e must be duplicated. Pindzola[1] has specifically derived the same parameter for constant δ_e, and Kawamura[6] derived it earlier for application to the structure and strength of the jet shock reflections and the transmitted shock waves. This parameter ξ can be used for approximating the jet characteristics without the need for duplicating γ_e, but its limitations must be mentioned. Since linearized theory was used, there will be errors at large values of p_e/p_∞. The magnitude of the difference in $\Delta\nu$ as p_e/p_∞ is increased for constant ξ and various combinations of γ_e and M_e for $M_\infty = 0$ is shown in Fig. 2 (from Ref. 1). If M_e is not matched, the Mach numbers within the jet will also be incorrect. It follows that the jet boundary variation beyond δ_e will not be correct. Unfortunately, there are almost no experimental data to verify the range of applicability of ξ to tests where the external properties of the jet are pertinent. It has been suggested[7] that much improved correlation at high values of p_e/p_∞ can be obtained at $M_\infty = 0$ by simply substituting the Mach number just downstream of the Prandtl-Meyer expansion fan (Fig. 1) for M_e in the simulation parameter.

All of the foregoing is based on the assumption that $M_e > 1$; for a sonic nozzle, ξ based on M_e does not apply, and both M_e and γ_e must be matched for correct simulation. However, ξ based on the Mach number downstream of the Prandtl-Meyer fan should still be valid when $M_e = 1$ provided that $p_e/p > 1$.

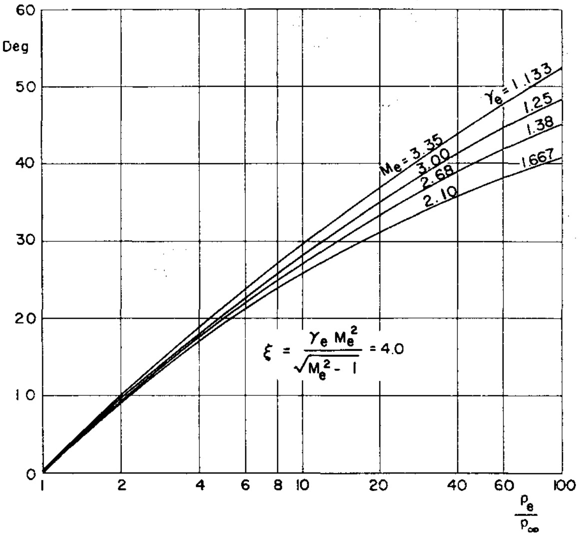

Fig. 2 Variation of $\Delta\gamma$ with p_e/p_∞ for various combinations of M_e and γ_e with $\xi = 4.0$ and $M_\infty = 0$.

Simulation Requirements for Jet Internal Properties

In jet impingement experiments, the jet internal properties must be examined; Pindzola[1] has indicated that, with p_e/p_∞, γ_∞, M_∞, and $(RT)_\infty$ matched, and with the nozzle exit area A_e to the same scale as the rest of the test article, the simulation parameters are

Mass flow = $\gamma_e M_e^2/(RT)_e$
Kinetic energy = $\gamma_e M_e^2 (RT)_e$
Internal energy = $(RT)_e/(\gamma_e - 1)$
Enthalpy = $\gamma_e (RT)_e/(\gamma_e - 1)$
Momentum and thrust = $\gamma_e M_e^2$

where the gas constant R is the universal gas constant divided by molecular weight. The immediate conclusion is that $(RT)_e$, M_e, and γ_e must all be matched simultaneously if simulation of all parameters is desired. There is some experimental evidence[2, 3] that $(RT)_e$, unlike γ_e, does not affect the position of the exit and transmitted shock waves. Experimental evidence concerning the relative importance of the various parameters for simulation of jet impingement effects is lacking, but it is basic that jet interference forces will be proportional to the dynamic pressures in the jet. Thus, there is a requirement for matching $\gamma_e M_e^2$, or jet momentum and thrust. Having done this, it is not possible also to match ξ simultaneously unless γ_e and M_e are individually duplicated.

Experimental Techniques

Let us now briefly examine the various techniques used or proposed for jet simulation:

Cold air: This common method is convenient operationally but can duplicate only M_e.

Cold helium: This has been used in some experiments[2] in order to utilize the high R (i.e., low molecular weight) to simulate $(RT)_e$ corresponding to ramjet exhausts, but γ_e, at 1.66, is grossly mismatched, and He is expensive.

Cold carbon dioxide: CO_2 duplicates γ_e well for both ramjet and rocket exhausts and has been used to simulate jets,[2, 3] but $(RT)_e$ is even lower than for air. Also, CO_2 has a relatively high liquefaction temperature, which limits its use to low values of M_e and p_e/p_∞.

Cold-gas mixtures: A 46% H_2, 54% CO_2 mixture (by volume) gives the same $(RT)_e$ as for cold helium for ramjet exhaust simulation.[2] This mixture is an improvement over He, in that γ_e is 1.40, but is still above the desired 1.27. Unburnt H_2 is an obvious safety hazard, and CO_2 is limited as previously noted. Tempelmeyer[8] presented analytical solutions for three-component cold-gas mixtures which simultaneously duplicate all three parameters (γ_e, M_e, and $(RT)_e$). The mixtures include hydrogen (5 to 20% by weight), a light hydrocarbon (ethane, methane), and a third component, which varies all the way from He to Freon 12. The cold mixtures can be applied only to turbojet temperatures (1650° R), but extension to rocket exhaust temperatures is possible with only modest heating of the mixture.[8] Careful mixture selection is necessary to reduce the flammability. Experimental experience with this method is still lacking.

Hot air: Hot air seems a logical choice for simulation, because its γ_e and $(RT)_e$ closely resemble those for various jet exhausts at the same temperatures. However, it is much easier to heat a jet through a combustion process; hence, hot air has seen little use.

Hydrogen peroxide: Decomposition of 90%-strength H_2O_2 has been used extensively by NASA as a turbojet exhaust simulator (Fig. 3).[9] Values of γ_e and $(RT)_e$ achieved approach those required for ramjets. This system has advantages due to its compactness (small supply lines minimize support interference effects), ease of operation (p_e is controlled by varying H_2O_2 weight flow), and the fact that the products (steam and oxygen) allow safe operation in a wind tunnel.

Hydrogen and air: Burning H_2 and air was also used[2, 3]; γ_e and $(RT)_e$ duplication for a ramjet are quite good, but this method lacks the other advantages of H_2O_2.

Turbojet simulator: A turbojet combustor[10] using air and a hydrocarbon fuel gives excellent simulation of turbojet and ramjet exhausts.

Scaled rocket motors: In order to duplicate high values of $(RT)_e$, models of the rocket motor using the same propellants as the full-scale motor, either solid or liquid, have been used quite successfully.[11–13] The major disadvantages are complexity[12] and the potential hazard to the wind tunnel.

Recommendations

From the foregoing it is concluded that there are two main cases of interest for jet interference: 1) when the jet external properties in the near field to the exit predominate, and 2) when both the internal and external jet properties for the entire field are important. The first case generally applies when the jet exits are well downstream on the aircraft or missile; problem areas are base drag, base recirculation, interference with the external flow near the base (particularly on adjacent control surfaces), and exit shock wave interference on other vehicle components. Case 1 can be handled adequately in most instances by duplication of p_e/p_∞ and ξ, with possibly a substitution of the Mach number just downstream of the Prandtl-Meyer expansion fan for M_e at high p_e/p_∞. Experimental simulation methods using a cold-air jet should be satisfactory.

Case 2 generally applies in those instances where the jet exits are upstream from the aft end of the vehicle, and therefore, the jet far field, both internal and external, must be correctly simulated. Typical examples are those where the jet boundary introduces significant interference effects and where any jet impingement is involved. The parameters to be individually duplicated are p_e/p_∞, γ_e, M_e, and $(RT)_e$. The most promising experimental approach for covering the full range of turbojet to rocket exhausts appears to be the three-component gas mixtures,[8] particularly if $(RT)_e$ duplication is not necessary, but this technique still remains to be proved in actual practice. Among proven techniques, H_2O_2 decomposition[9] is recommended for turbojet and ramjet simulation, and scaled rocket motors are best for rocket exhaust simulation.

Rocket Booster Base Heating

Rocket boosters employing multiple engines have complex flow patterns in the base region, which are influenced by the booster Mach number-altitude trajectory, the number and spacing of the rocket engine nozzles, the booster skirt configuration, and, when applicable, the introduction of turbopump exhaust products. For certain combinations of these factors, the exhaust will recirculate into the base region, and base burning may also occur. The base heating that results has been credited with causing some early missile failures. The complexities of base recirculation problems were revealed in the flow studies of Goethert and Barnes.[5] A theoretical treatment was presented by Goethert[14] for the four-nozzle cluster case, and Page and Dixon[15] subsequently gave a more general treatment for three or more nozzles. However, the complex nature of the problem has generally made it necessary to rely on experimental evaluation for each booster configuration. The experimental techniques employed are critical, because scaled models must be used to represent a phenomenon which includes all modes of heat transfer plus combustion in the area of interest. These techniques may be divided into two basic groups according to duration: long, if test time is measured in seconds, or short, for a test period measured in milliseconds.

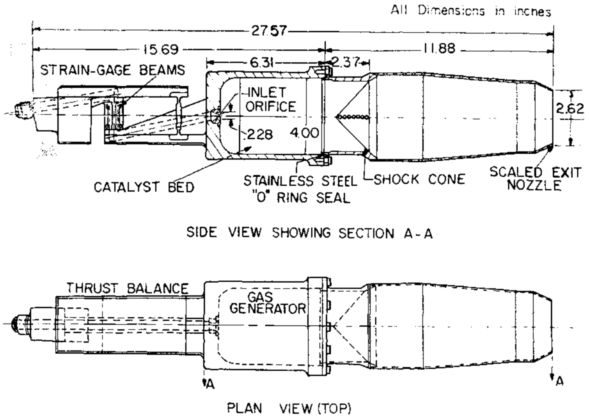

Fig. 3 Details of hydrogen peroxide generator and thrust balance system.

Long-Duration Technique

The long-duration technique has been used with both cold air and hot exhausts provided by standard rocket propellants. The cold flow method was used quite successfully in defining the basic flow patterns.[5] The simulation parameters used are identical to those discussed previously for duplication of δ_e in Fig. 1; excellent agreement of peak base pressures was shown.[14] Qualitative indication of the base flow was obtained by releasing smoke or other tracers (e.g., mica particles) from various locations near the base. However, to measure heat transfer, it is necessary to simulate the hot exhaust by operating a scaled rocket propulsion system in the wind tunnel. Full jet duplication can be obtained by using the same propellants, combustion chamber pressures, and nozzle area ratios as the full-scale vehicle. Liquid engines require complex fuel systems, controls, and plumbing,[12] but they do offer the advantage of rapid, successive firings by remote control. Solid rockets require a tunnel shutdown and propellant replacement for each firing but are simpler.

Some of the complexity of a base-heating model is evident in Fig. 4, which shows a recent Titan III installation at the Arnold Engineering Development Center (AEDC) in which both the solid and liquid motors were fired simultaneously. This model is supported by the conventional method with a strut, through which necessary plumbing and wiring are brought into the model. The strut offers the opportunity of pitching the model, but it represents an undesirable aerodynamic interference, particularly at transonic speeds. Normal practice is to locate the strut as far upstream of the model base as possible, consistent with wall-reflected shock wave considerations.

An installation technique[16] that eliminates the need for the support strut, at the expense of pitch angle variation, is shown in Fig. 5. The model is cantilevered from upstream

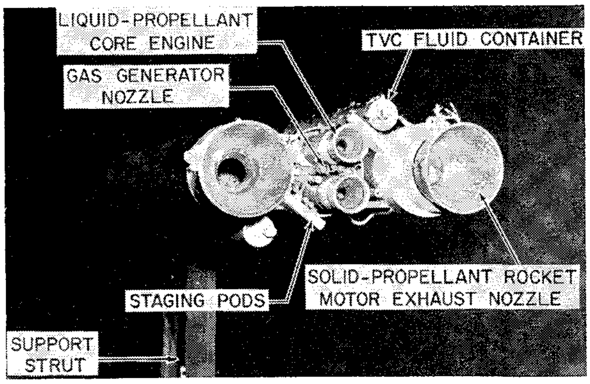

Fig. 4 Rear view of Titan III strut-mounted base heating model.

of the tunnel throat and is contoured through the nozzle region according to stream tube requirements. For $M_\infty = 4$ testing, for which the model area reduction at the throat would be excessive using the stream tube design, the method of characteristics is used to define the model shape in conjunction with an existing, lower Mach number nozzle. This type of installation maximizes model size for a given air handling capacity, since reflected shock wave interference is eliminated and thermal choking is avoided by diverging the diffuser walls.[17] Perforated walls and suction have also been used to attenuate reflections of the jet exit shock and waves caused by model protuberances into the exhaust plume.

Heating rates are usually measured by slug-type calorimeters, using the equation for transient heating

$$\dot{q}/A = \rho\tau c\, dT/dt \qquad (1)$$

where $\dot{q}$ is the heat-transfer rate in Btu/sec, A the area exposed to the heating, and ρ, τ, and c are the density, thickness, and specific heat of the calorimeter material, respectively. It is generally desired to measure both the convective and radiative contributions to base heating separately. Calorimeters are subject to quite a variety of inaccuracies[18, 19]; hence, considerable care must be used in their design and calibration. Some of the important features are: 1) the calorimeter should approximate the temperature history and duplicate the contour, roughness, and, if possible, emissivity of the surface it replaces; 2) mounting insulation must not generate large losses due to conduction to the insulation; and 3) heat losses from the rear face must be minimized by proper insulation.

Figure 6 shows examples of calorimeters which tend to meet the desired design features. The total heat calorimeter (Fig. 6a) is of the same material as the remainder of the base. The cap, which minimizes heat loss from the rear face of the insulated calorimeter section, should be of low mass and high conductivity; it should also be externally insulated, if possible. The spherical, convective-heat-transfer calorimeter (Fig. 6b) is intended for instream measurements in regions adjacent to locations of temperature-sensitive equipment in the full-scale vehicle; its spherical shape eliminates the measurement dependency on the uncertain flow direction. The radiant calorimeter[19] (Fig. 6c) has an aperture sized to accept radiant heat but to prevent external convective currents from appreciably influencing the cavity temperature history. The sides of the aperture walls are carefully polished to maximize the viewing field, which should approximate 180 degrees.

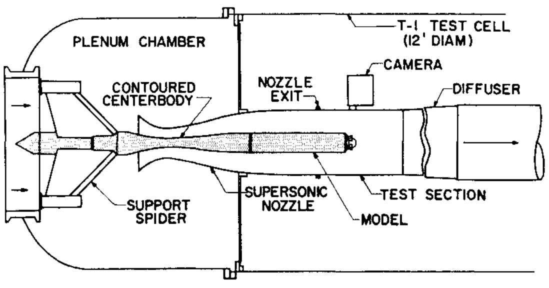

Fig. 5 Tunnel installation for contoured base heating model.

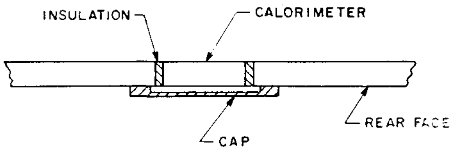

a) TOTAL HEAT CALORIMETER FOR BOOSTER BASE (REF. 18)

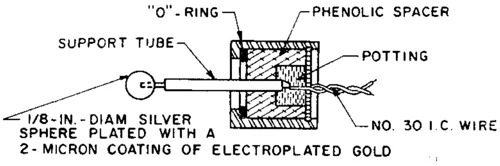

b) CONVECTIVE HEAT CALORIMETER FOR IN-STREAM MEASUREMENTS

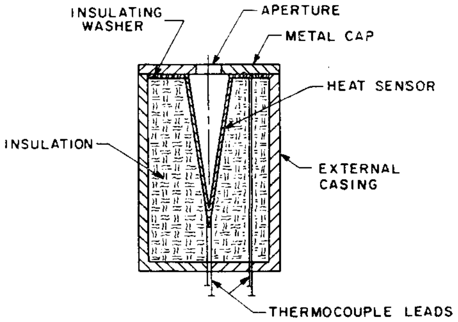

c) BLACK BODY CAVITY-TYPE RADIANT HEAT CALORIMETER (REF. 19)

Fig. 6 Schematics of various calorimeter designs.

One method commonly used for defining the radiative heat component is to place two slug-type calorimeters (Fig. 6a), one with a highly polished surface and the other with a blackened surface, adjacent to each other. The difference between the indicated heat rates is then roughly the source of radiant heat rate. Unfortunately, it is very difficult to maintain the polished surface in a rocket exhaust environment and to minimize convection errors on both units; theoretically, the black-surface unit can be covered by a transparent shield, but this, too, has obvious limitations.

In view of such problems associated with individual slug-type calorimeters, there is some trend toward simply measuring the combined convection and radiation effects by imbedding thermocouples at various points in the base to obtain local heating rates. Base heating is generally very nonuniform; this approach would eliminate the thermal flow distortions caused by insulated slugs.

Short-Duration Technique

The Cornell Aeronautical Laboratory[20–25] has developed an approach to the study of base heating (Fig. 7) employing techniques similar to those in use for shock tubes. The concept is that rocket exhaust flows need be duplicated only for that length of time sufficient to establish steady flow

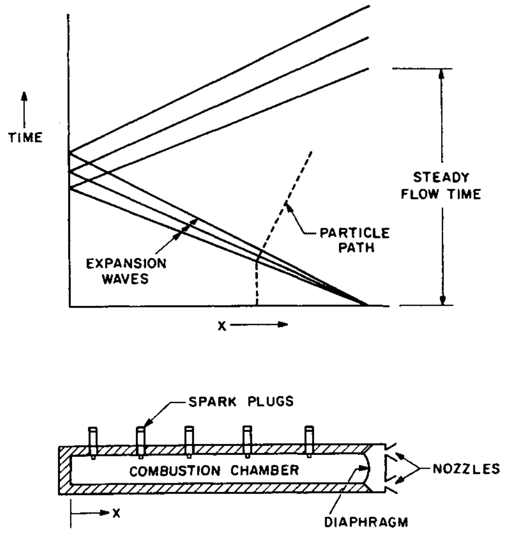

Fig. 7 Constant-volume combustor, short-duration flow generator.

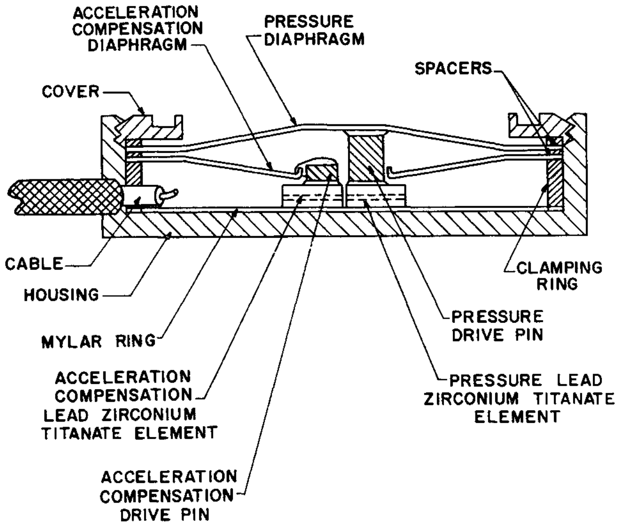

Fig. 9 Cross section of lead zirconium titanate transducer.

patterns. The first successful experimental results were obtained without external airflow by discharge into an altitude chamber.[21, 22] Composition, pressure, and temperature were duplicated for a few milliseconds. The constant-volume combustor is loaded with an appropriate gas mixture, which is ignited, causing the diaphragm to rupture at a predetermined pressure. Steady-state flow is obtained during the time it takes the expansion wave generated by the flow out of the combustor to travel to the upstream end of the tube and return; for a 15-ft length, the testing time is as much as 5 msec. Time histories show good repeatability for the combustion process (Fig. 8). The pressure decap is caused by heat loss to the walls; this deficiency was corrected in later technique refinements.[25]

Thin-film resistance thermometers[23] are used to measure total heating rate and radiative heating alone. A 0.1-μ film of platinum, approximately 1 mm wide and 5 mm long, is deposited on a small Pyrex slab that can be inserted in the model. A radiation gage is made by adding a layer of Pyrex over the platinum surface. The one-dimensional theory of heat conduction in a homogeneous body is used to relate the surface temperature history to the heat-transfer rate. Pressures are measured by piezoelectric-type transducers[24] using lead zirconium titanate crystals (Fig. 9). These transducers have a large range of linearity, a high sensitivity (1500 mv/psi), acceleration compensation, and frequency response in excess of the requirements for short-duration testing. Repeatability of the reduced data is indicated in Fig. 10.

The short-duration technique is also in use at NASA George C. Marshall Space Flight Center and NASA Lewis Research Center, in both altitude chambers and conventional wind tunnels. In the latter case, a remotely controlled system for charging the combustor and the use of quick-opening valves (instead of diaphragms) has made it possible to achieve firings in quick succession.

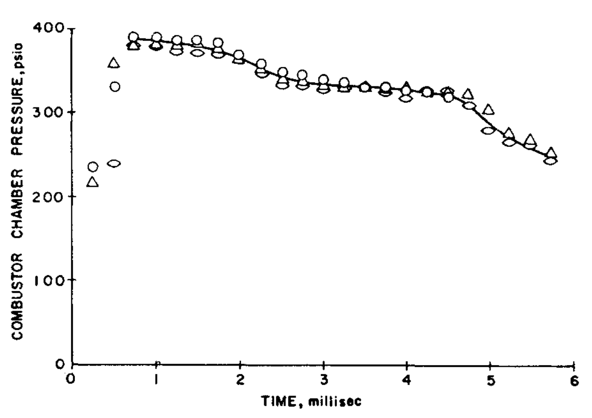

Fig. 8 Combustor chamber pressure variation, with time for three runs of Fig. 7 model.

The problem of obtaining valid data in the short-run time was fully recognized from the beginning by Weatherston and Hertzberg.[20] Ihrig and Korst[26] raise the question of stabilization times required for mass and heat transfer. They show that transport phenomena require significantly longer times to reach equilibrium than do those governed by wave propagations. However, Rickard and Dennis[27] report that the time required for heat-transfer stabilization is about the same as for pressure stabilization and within the available test time. Their basic flow pattern is one of reverse flow into the cluster center, which has the stabilization mechanism of a wave process. Clearly, the short-duration method would be inappropriate for cases involving base burning, long-range burning propagation effects, or pulsations. The probability of such effects normally decreases with alti-

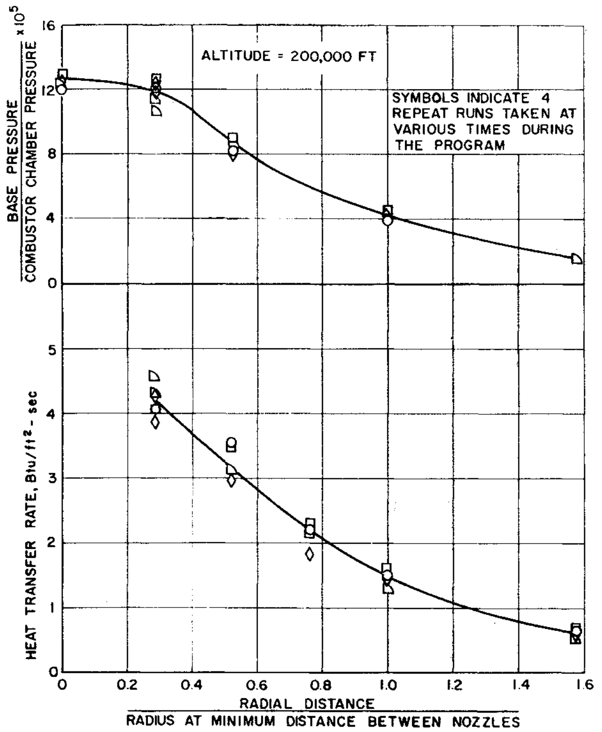

Fig. 10 Repeatability of data from Fig. 7 model.

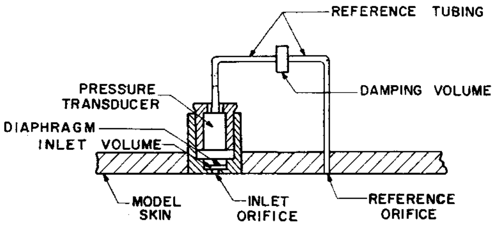

a) OFF-SET REFERENCE PRESSURE

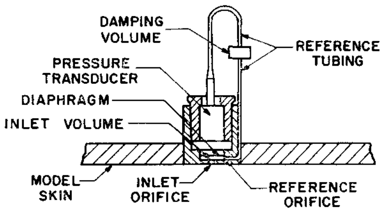

b) INLET VOLUME REFERENCE PRESSURE

Fig. 11 Details of pressure transducer cell installation for two reference pressure systems.

tude, which may have a bearing on where the short-duration technique is most valid. Obviously there is a need for precise experiments correlating the two techniques.

Scaling

The foregoing problems seem minor compared to our lack of understanding of scaling laws. Beheim and Obery[28] have discussed many of the scaling problems that arise in the long-duration technique when liquid propellants are used. Difficulties in scaling combustion phenomena are well known. One technique used at the Arnold Engineering Development Center, in an attempt to approximate the full-scale case of possible base burning due to turbopump exhaust, is to substitute hydrogen for the actual combustible exhaust products. Since H_2 has wide flammability limits and high flame speed, combustion has a greater chance of occurring during the shorter gas residence time in a model base. The hydrogen (plus inert gas if needed) momentum per unit area and heat of combustion for a scaled model are matched to the full-scale vehicle.

Radiation measurements in a model will be low because the distance for jet afterburning, which is a main contributor to radiation, is too long in terms of model scale.[28] Fortunately, radiation effects are usually small compared to convective. If necessary, one possible method of improving the accuracy of the measurements is to determine the trend along the trajectory in wind-tunnel tests and obtain the proportionality factor from the results of full-scale firings at sea level. Page and Dixon[15] have also shown that a large error in convective heat rates is possible with models. For example, a $\frac{1}{10}$-scale model is shown (analytically) to produce rates nearly three times those for the full-scale vehicle.

It must be concluded that the direct application of heat-transfer rates measured on models to the full-scale vehicle is a poor approximation, which probably grows worse with decreasing model scale. However, relative results for different configurations and trends due to changes in test conditions are still useful. Fortunately, base heating is a yes or no condition for a large part of typical flight trajectories. Since the presence or absence of substantial base heating is mainly dependent on the fluid dynamic aspects of the problem, which can be correctly scaled, this portion of the results is directly applicable to the full-scale vehicle. Even if base burning does not occur in the model, its probability at full scale for the same test conditions could be assessed by base area gas sampling. Therefore, model tests are particularly applicable where the test objective is to eliminate or postpone base heating.

Transonic Pressure Fluctuation Measurement and Prediction

The problem of buffeting is at least as old as compressibility effects in subsonic aircraft. Since missile and space vehicle designers persist in using sharp corners, the same basic aerodynamic problem appears in these vehicles but with greater intensity. Several rockets have failed during the transonic and low supersonic range of their exit trajectories, and it is suspected that the combination of unsteady aerodynamics and maximum dynamic pressures occurring at transonic speeds has led to buffeting loads that contributed to some of the failures. Consequently, there have been numerous wind tunnel tests at both NASA and AEDC on specific missile and space systems to determine the nature and magnitude of the flow fluctuation phenomena.[29–32] To the designer, there would appear to be two major effects of the pressure fluctuations, namely, 1) local surface loading and dynamic behavior, and 2) integrated effects on the structure, including the dynamic response of the vehicle.

Local surface pressure fluctuations can be readily measured using conventional, flush-diaphragm, differential pressure transducers of $\frac{1}{2}$- and $\frac{1}{4}$-diam. The undamped natural frequencies of the diaphragms are ≥ 5000 cps. Pressure cell installations using two reference pressure techniques are shown in Fig. 11. The disadvantages of mounting the diaphragm directly on the model surface (mechanical damage and surface discontinuities) have been overcome with small loss of frequency response. The inlet volume and orifice diameter must be consistent with the desired frequency response; the acoustical natural frequency of the orifice-volume combination should preferably be above that of the transducer. The reference pressure is a highly damped mean of the unsteady pressure being measured, with the tubing sized to act as a low-pass acoustic filter. In the inlet volume reference pressure system, the reference pressure tubing should be small to minimize any effect on inlet volume. Dynamic calibration techniques are covered in detail in Refs. 33 and 34. In the latter, it is shown that the types of installations of Fig. 11 have excellent response characteristics even beyond 20% of the diaphragm natural frequency under some conditions.

Before proceeding with tests on models, pressure fluctuation characteristics of the tunnel airstream are calibrated and critical frequencies (if any) of the tunnel are established. The rms pressure variations measured at AEDC[35, 36] were generally less than 0.01 of stream dynamic pressure q_∞. A typical data acquisition system[30] uses magnetic tape recording; power spectral densities (frequency distribution of pressure fluctuation intensity) are obtained from the tape records using a wave analyzer.

Basic Aerodynamic Effects and Their Prediction

A study[37] of the fundamental aerodynamic phenomena of the flow just downstream of the shoulders of cone-cylinder bodies showed that at low subsonic Mach numbers the flow is separated aft of the shoulder, subjecting the cylindrical region to random fluctuations due to separation. As M_∞ is increased, the flow becomes attached at the shoulder and a shock wave appears on the cylinder, usually with separation aft of the shock wave. The shock wave oscillation will result in appreciable local fluctuations. As M_∞ approaches 1.0, the shock wave moves downstream, and only the small pressure fluctuations associated with boundary layer noise remain. By far the greatest pressure fluctuations aft of the shoulder are caused by alternating flow separation and attachment. Chevalier and Robertson[37] have shown that the ΔM_∞ over which the alternating flow occurs is always ≤ 0.05 and usually <0.03. The amplitude and the Mach number range of occurrence increase with both angle of attack (leeward side) and cone angle. Amplitudes can be predicted by the differences in the static pressure distributions of the separated and attached boundary-layer cases taken at nearly the same M_∞ (Fig. 12). These results indicate that, as far as the largest local effect is concerned, it may often be possible to avoid difficult direct measurements by applying such prediction techniques.

Scaling Parameters

As with any aerodynamic problem involving boundary-layer effects, the Reynolds number is an important parameter. An increase in model scale (and *Re*) results in attachment of the boundary layer aft of the cone-cylinder juncture at lower M_∞.[38] The large fluctuations due to the alternating attached and separated flow also occur at lower M_∞ with increasing model size (and *Re*).[31] A very definite *Re* effect on the magnitude of the rms pressure coefficient fluctuation $(\Delta C_p)_{\text{rms}}$ was noted for models of different size[31] and for the same model.[32] In the latter case, the values of $(\Delta C_p)_{\text{rms}}$ level off at $0.75 \times 10^6 < Re < 3.4 \times 10^6$, where *Re* is based on the local model diameter. Reference 32 also further reinforces the evidence that scale effects are due to absolute rather than unit *Re* in the approximate agreement in peak values of $(\Delta C_p)_{\text{rms}}$ obtained at the same absolute *Re* (0.75×10^6) for models which differed by a factor of 5 in scale. Thus extrapolation of wind-tunnel pressure-fluctuation experiments to the full-scale vehicle is questionable unless the *Re* based on local diameter is at least 2 or 3×10^6.

The scaling parameters for the experimentally determined frequencies and power spectral densities are also needed by the designer. The power spectral density $F(\omega)$ is normally obtained as a function of frequency from a wave analysis of an individual pressure record and is defined by the following equation:

$$(\Delta p_{\text{rms}})^2 = \int_0^\omega F(\omega)d\omega = \int_0^f 2\pi F(\omega)df \qquad (2)$$

where Δp_{rms} is the rms amplitude of a pressure deviation about a reference pressure, and ω and f are the frequencies in radians and cycles per second, respectively. The scaling parameters suggested are

$$f_{FS} = f_M(D_M/D_{FS})(V_{\infty FS}/V_{\infty M}) \qquad (3)$$

and

$$F(\omega)_{FS} = F(\omega)_M(q_{\infty FS}/q_{\infty M})^2(D_{FS}/D_M)(V_{\infty M}/V_{\infty FS}) \qquad (4)$$

where D is reference diameter, and subscripts FS and M refer to full-scale and model. These parameters were developed[39] from dimensional considerations; the one for frequency simply specifies a constant reduced frequency or Strouhal number. Jones and Faughner[32] have demonstrated good correlation of the scaling parameters at the full-scale case for different combinations of two model sizes and two working fluids (air and Freon) at constant *Re* and M_∞.

Measurement of Integrated Effects

Integrated effects of pressure fluctuations, particularly as they are reflected in bending moment variations at critical vehicle sections, are important in design. The most straightforward method is a pressure integration technique used by Cole.[40] Pressure transducers are placed over the entire surface forward of the moment reference station, and each is assigned an area-moment segment of the model and adjusted for sensitivity accordingly. The time-correlated signals are summed electrically to give the desired bending moment fluctuations. However, the instrumentation requirement is formidable.

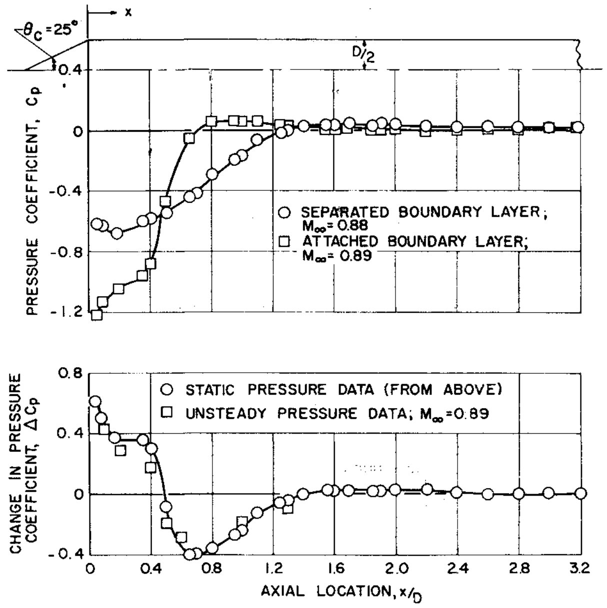

Fig. 12 Comparison of predicted and measured peak-to-peak pressure fluctuations at zero angle of attack.

One promising method (under development by the Martin Marietta Corporation) for a more direct measurement of the integrated aerodynamic excitation is known as the inertia-compensated balance technique (Fig. 13). Unlike pressure transducers, a conventional internal strain gage balance is inertia sensitive in the frequency range of interest. The motion of the model in response to the aerodynamic excitation tends to influence the desired output signal at a moment gage, whereas the coupling of the sting and support system will also produce undesired moment readings due to the model inertia. An accelerometer is positioned within the model, so that its output, combined with that of the moment gage, matches a known arbitrary input $F_A(t)$ which represents the aerodynamic excitation. Simultaneously, the accelerometer location must be such that the same combined output due to any sting coupling represented by $F_C(t)$ shall be zero. (A more complex form of the balance employs two sets of accelerometers and moment-measuring stations, but it is possible to match the required outputs exactly with only one set. Two sets permit determination of the normal force fluctuations as well as transfer of the moment variations to another station.) Very flat response vs frequency characteristics has been demonstrated, with less than 10% deviation at the resonant frequencies of the model and sting support system. Excellent agreement in the moment power spectral densities with those from the pressure integration technique has been obtained in one case.

After either the pressure-integration or the inertia-compensated-balance technique has been used to measure the

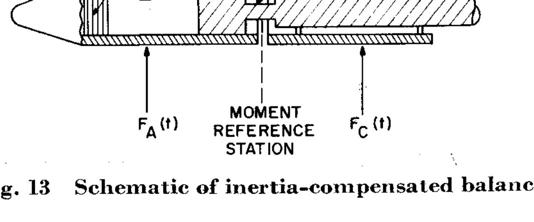

Fig. 13 Schematic of inertia-compensated balance.

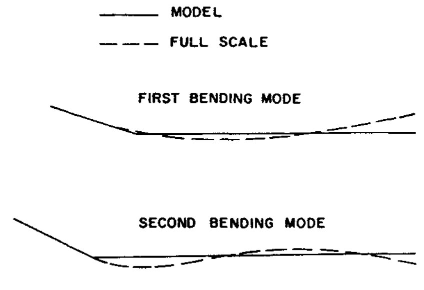

a) APPROXIMATION OF BENDING MODES

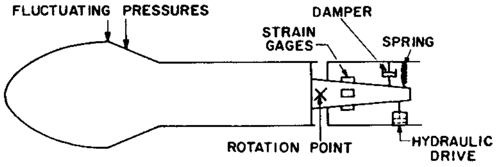

b) SCHEMATIC DRAWING OF DYNAMIC MODEL INSTALLATION

Fig. 14 Dynamic-response model technique.

aerodynamic forcing function, the next step is to determine the dynamic response of the vehicle to this forcing function. Cole[40] has demonstrated a method of direct dynamic response measurement, which is shown schematically for a hammerhead configuration in Fig. 14. An approximation of the first and second bending modes is obtained by a single rotation point, about which the model can be oscillated in either the free or forced method. Sting coupling effects are minimized by making the model as light as possible. Excellent agreement with a calculated value of the peak moment power spectral density was demonstrated. The possibly critical nature of the dynamic response for this configuration was also clearly shown in the large differences between the moment power spectral densities measured dynamically and the aerodynamic input obtained with a rigid model by the pressure integration technique. The possible inaccuracies of this method are the bending mode approximation and the lack of complete compensation for sting and support system interaction, particularly at the sting critical frequencies. It is apparent that there is a need for further technique development, such as the use of dynamically scaled models wherein the inertia effects of the model are included in the measured moments but those due to sting and support system coupling are not.

Dynamic Stability Investigations

There is an ever-increasing requirement for determination of the dynamic stability derivatives of aircraft and aerodynamic missile configurations at transonic and supersonic speeds because of the trends to both higher density designs and to increasing mass concentration in the fuselage. Ballistic re-entry vehicles already have these same characteristics without the benefit of aerodynamic control surfaces, and hence potentially have an even more critical dynamic stability problem.

The earlier work on sting-mounted models was mainly concentrated on the free-oscillation single-degree-of-freedom technique because of its relative simplicity and economy.[41, 42] Most designs in this category consist of a cross flexure for model rotation to avoid the internal damping of bearings, a triggering mechanism, an oscillation arrester for use in cases of instability, and a means of measuring the instantaneous angular displacement, from which the frequency and rate of oscillation decay are obtained. The single-degree-of-freedom technique using such a balance is capable of measuring the moment derivatives that arise from all three angular motions, i.e., the rates of change of rolling moment coefficient with respect to angular velocity in roll $C_{l_{\dot{\varphi}}}$, of pitching moment coefficient with respect to both pitch and angle of attack angular velocity $(C_{m_{\dot{\theta}}} + C_{m_{\dot{\alpha}}})$, and of yawing moment coefficient with respect to both yaw and sideslip angular velocity $(C_{n_{\dot{\psi}}} - C_{n_{\dot{\beta}}})$, as well as the static displacement derivatives $C_{l_{\varphi}}$, $C_{m_{\alpha}}$, and $C_{n_{\beta}}$. However, the free-oscillation technique has certain basic deficiencies, namely, the difficulty of obtaining data under conditions of dynamic instability, the reduction in angular travel when α (pitch) or β (yaw) ± 0 because of the static displacement of the model caused by the pitching and yawing moments, and the inconvenience of obtaining nonlinear amplitude and frequency effects.

Forced-Oscillation Technique

Forced-oscillation systems[43–46] will overcome the deficiencies of free-oscillation systems and therefore are extensively used, particularly in the transonic and supersonic speed ranges. Figures 15 and 16 are balance sketches from Refs. 44 and 46. Both cases use a crossed flexure pivot. Angular displacement is sensed by strain gages on the flexure pivot and the moment is measured between the pivot and the actuating mechanisms, which consist of an externally supplied hydraulic cylinder and restoring spring in the first case, and a push rod mechanically driven by an electromagnetic shaker housed at the rear of the sting in the second case. The amplitude of oscillation is controlled by feed-back loops, in which the frequency is controlled by the hydraulic pump motor speed and the shaker frequency. For maximum accuracy and simplicity, these systems are usually operated at their undamped natural frequencies, so that the measured moment is exactly 90° out of phase with the displacement and consists of the damping moment alone. Natural frequency variation is obtained either by using cross flexures of different stiffness or by a spring change (such as the coiled frequency spring of Fig. 15), with the boundary condition that the model natural frequency always remain well below that of the sting support in either direction. It is actually not necessary to operate at resonance, since electronic resolvers can be provided to separate the moment into com-

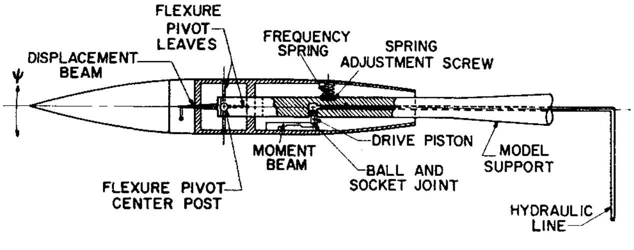

Fig. 15 NASA-Langley forced-oscillation balance and drive system.

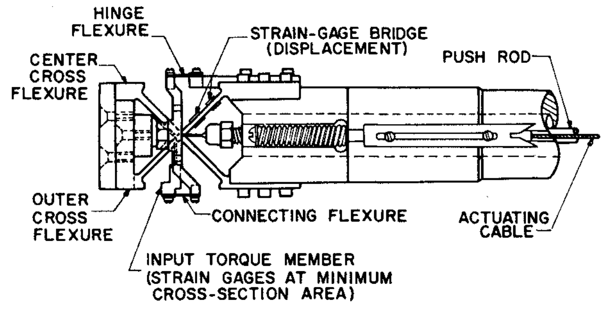

Fig. 16 AEDC-VKF small-amplitude, flexure-pivot forced-oscillation balance.

ponents in phase and 90° out of phase with the displacement.[44] Another advantage of the forced-oscillation technique is that random effects such as airstream turbulence or buffeting have zero net input to the measurements.

The balance described by Beam[43] is unique in that the axis of oscillation was varied to produce combined roll and pitch or roll and yaw. Thus it was possible to determine the cross derivatives $C_{n_{\dot{\theta}}}$ and $C_{l_{\dot{\psi}}} - C_{l_{\beta}}$ (rate of change of yawing moment coefficient with roll angular velocity and of rolling moment coefficient with yaw and sideslip angular velocity), as well as the static displacement derivative $C_{l_{\beta}}$.

All of the balances previously described are limited in maximum amplitude because of stress limits on the pivot flexures. This problem can be circumvented by the use of a ball-bearing pivot, at the expense of introducing bearing damping, which may be large in comparison to the aerodynamic damping and is characteristically of poor repeatability. The ball-bearing pivot design of Fig. 17[47, 48] eliminates this bearing friction problem by use of an A-frame type of moment-sensing unit situated between the ball-bearing pivot and the model attachment surface. (This is a modification of a design developed at NASA Ames Research Center; it is also similar in principle to that given in Ref. 45.) It is in use at AEDC for sting-mounted ballistic configurations up to full-scale sizes with oscillation amplitudes up to ±15°.

Large-Amplitude Systems

When amplitudes greater than ±15° are desired for ballistic shapes, one must mount the model on a strut or transverse rod.[49, 50] The model is free to rotate about the rod on two very-low-friction, instrument-type bearings contained within the model; ±90° of motion is possible. The principal measurement is either a photographic time history of the motion or a history obtained by use of an angular transducer[49] which does not depend on mechanical contact between the fixed and moving parts of the transducer. The models must be statically stable. The obvious disadvantages of these systems are the bearing friction and the possibility of aerodynamic interference from the supporting structure, particularly in the transonic range. As M_∞ increases, the small aerodynamic damping moment becomes even smaller and hence more difficult to measure. One means of reducing frictional torque is to replace the ball bearings with gas bearings (cylindrical journal bearings using high-pressure gas as lubricant).[51, 52] Gas bearings have less than 0.2 of damping parameter of ball bearings for comparable load-carrying capacity, which exceeds 300 lb in the radial direction.[51] A comparison of the damping data[52] obtained from a transverse-rod-mounted blunt cone (with boat-tail) model using gas and ball bearings is presented in Fig. 18. The data are corrected for bearing friction, which is also shown separately. The ball-bearing damping data are uncertain to within a factor of 2, whereas the gas bearing results are more accurate. The bearing damping comparison would be even more extreme at higher tunnel dynamic pressures, since the gas-bearing damping is roughly independent of applied load and would vary inversely with dynamic pressure.

Free-Flight Technique

A promising technique for dynamic stability testing without support interference is the use of freely flying models.[52, 53] Typical construction is a lead core and a plastic foam exterior shell, which maximizes the ratio of mass to moment of inertia and thus also the number of oscillations within the field of view of the camera. The model is supported at the upstream end of the test section by a wire that passes through it. After flow establishment, an impulse tension load is applied to the wire, causing it to break at a notch inside the model and thus free the model. The initial α can be readily varied by adjustment of the wire angle with respect to the model base. A further refinement (in use at Jet Propulsion Laboratory and Arnold Engineering Development Center) consists of a compressed-air gun downstream of the test section from which the model is launched upstream, with velocity just sufficient to reach the forward edge of the viewing area. This effectively doubles the amount of data compared to the wire-supported system and will permit protection of the model from high-temperature ambient conditions before launch, if necessary. Motion pictures at 4000 frames/sec typically give several hundred frames covering three to six cycles of oscillation. Dayman[53] outlined additional potential uses of this technique for measurements of drag, base pressure (utilizing telemetry equipment that must withstand accelerations roughly three orders of magnitude less than in a ballistic range), and wake shape.

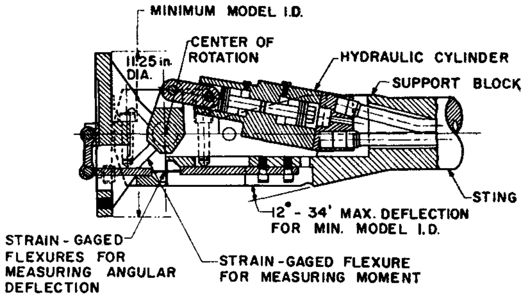

Fig. 17 **AEDC-PWT ball-bearing type of forced-oscillation balance.**

Simulation Requirements

The two main simulation parameters pertinent for dynamic stability measurements are *Re* and the Strouhal number, $\omega l/2V_\infty$, where ω is the angular velocity and l is the characteristic length. Since V_∞ is usually approximately duplicated through duplication of M_∞, ωl must be kept constant. There is very little experimental evidence concerning the sensitivity of the dynamic damping parameters to Strouhal number at supersonic speeds; only small effects were noted in both pitch and yaw for an airplane configuration at transonic speeds.[45] Since Strouhal numbers generally decrease with increasing M_∞, it is reasonable to expect reduced sensitivity to approximate duplication at higher M_∞. One area where care is indicated is for those shapes subject to flow separation ahead of the base, such as sharp-cornered and flared ballistic shapes at transonic and low supersonic speeds.

The nature of an aerodynamic body oscillation, particularly at the high amplitudes desired for ballistic shapes, frequently involves flow separation. Thus, the state of the boundary layer should be duplicated if possible. This requires that the *Re* be sufficiently great to insure the turbulent case, which is most generally found in flight. The *Re*

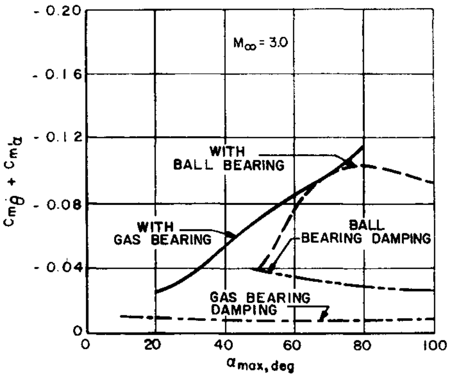

Fig. 18 **Comparison of pitch damping data with gas and ball pivot bearings.**

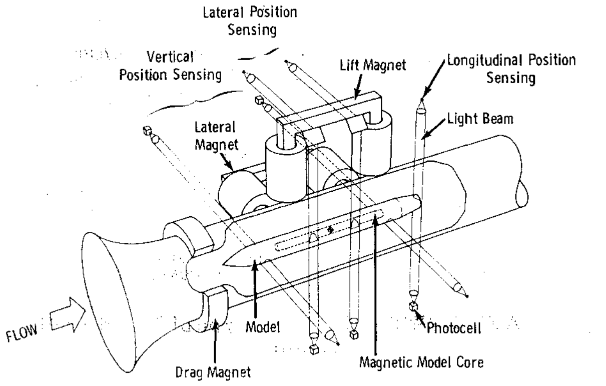

Fig. 19 **Schematic of a five-component magnetic suspension system.**

values mentioned for ballistic shapes in the section "Transonic Pressure Fluctuation Measurement and Prediction" are also believed to apply for dynamic stability work in the transonic range.

It is obvious from the foregoing that the useful captive-model dynamic-stability measuring techniques in wind tunnels all involve rotation in one degree of freedom. However, there is still a need to identify separately $C_{m_{\dot\theta}}$, $C_{m_{\dot\alpha}}$, $C_{n_{\dot\psi}}$, and C_{n_β}, particularly for aircraft configurations. A one-degree-of-freedom translation mechanism would give either $C_{m_{\dot\alpha}}$ or C_{n_β} alone, allowing $C_{m_{\dot\theta}}$ and $C_{n_{\dot\psi}}$ to be obtained by the combination of the rotation and translation techniques. The need for the continuation of the development efforts toward a successful translation mechanism is apparent. Also, it would appear that adaptation of the free-flight technique for the aircraft type of models would be most useful.

Magnetic Model Suspension

Complete elimination of the model support structure by the use of magnetic fields has been recognized as a potential solution to support-interference problems for some time.[54] However, it remained for Office Nationale d'Etudes et de Recherches Aeronautiques (ONERA) in France to develop and demonstrate the first successful magnetic suspension system in a wind tunnel in 1955.[55] Subsequent improvements in system dynamics[56] and application for model force measurements[57] have been reported. Base pressures were measured using optical manometer techniques.[58] Very similar magnetic suspension systems have been built and placed into operation at the University of Virginia[59] and at Massachusetts Institute of Technology.[60] A five-component system of larger load-carrying capacities is under construction at AEDC.

Basic Principles

The basic arrangement of a five-component suspension system is shown in Fig. 19. An iron rod in the center of the nonmagnetic model is suspended by three sets of magnets: 1) a horseshoe "lift" magnet in the vertical plane, arranged symmetrically to the model's center of gravity, which balances the loads due to gravity and lift (sum of forces exerted by each magnet leg) and pitching moment (sum of individual magnet leg forces with appropriate moment arm); 2) a similar "lateral" magnet in the horizontal plane to balance side force and yawing moments; and 3) an air core "drag" magnet mounted upstream of the model to balance the drag force. The desired model position within the test section is maintained very precisely by five position-sensing light beams (one for each corresponding magnet control system) that fall on photocells. The photocell voltage output, which is proportional to the light that passes the model and is absorbed by the cell, forms the input signal of the control system.

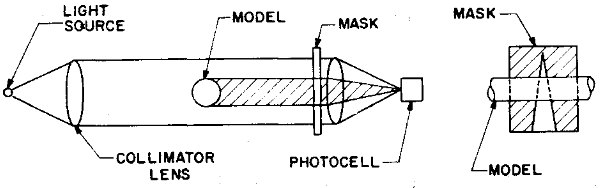

Fig. 20 **Extended range position-sensing system.**

For a given model position, the force $\bar{F}$ produced by the interaction of a magnetic field with the magnetic core of the model is in the general form

$$\bar{F} = \bar{M}(\nabla \cdot \bar{B}) \tag{5}$$

where $\bar{M}$ is the magnetic dipole moment of the core and is proportional to the magnetization caused by the various magnet systems, and $\bar{B}$ is the magnetic field. $\bar{M}$ approaches a constant and maximum value as the core approaches saturation, beyond which increases in magnet coil currents will essentially change only the magnetic field divergence $\nabla \times \bar{B}$. Operation with a saturated core will tend to eliminate interferences between the different magnet systems because of changes in $\bar{M}$.

The force F exerted by an electromagnet on a piece of magnetic material with distance x between the two varies with current as KI/x^n where the constant K depends on the geometry and magnetic properties of the core and magnet. For an unsaturated magnet, $n \approx 2$ if the model core is saturated or $n \approx 4$ if it is not. For an infinitesimal model motion ($\Delta x \rightarrow 0$) as an aerodynamic load is applied, $\Delta F \approx K\Delta I$. Thus it is apparent that a magnetic suspension system is fundamentally very statically unstable at constant I. A model displacement toward a magnet results in an increase in attractive force and a rapidly increasing displacement, with a similar result in terms of decreasing force in the opposite direction. Holmes[54] recognized the need for controlling I to obtain a stable equilibrium.

The control system[56, 59, 60] is the heart of the magnetic suspension concept. Basically, it must control large direct currents quickly enough to be consistent with the time lags due to the magnet and the model inertia. Phase-lead networks are used to produce a signal which is proportional to both the model deviation and its rate of change of deviation, thus permitting a rapid, stable response in the magnet. Adjustment to changes in steady-state loads is performed by an integrator circuit which integrates the error signal and maintains the new current output even when the error signal disappears.

A position-sensing system of the type shown in Fig. 19 allows only very small displacements and therefore very small pitch and yaw angles before the available system range is exhausted. Both ONERA and MIT have improved their sensing methods, so that the model is within reach of the system throughout most of the flow cross section. A large-diameter light beam and a V-shaped mask provide a wide displacement control range (Fig. 20). Any desired function can be obtained by proper mask shaping. Practically, the light beam should not be of larger diameter than required in order to minimize sensitivity decreases and light path perturbations caused by heat and shock waves.

Measurements and Limitations

Since the forces are extremely sensitive to position changes, and there can be significant interaction between the force components, a complete calibration must be made[61] for each α or β. The sensitivity of the forces to position also requires precisely repeatable location of the model with respect to the magnets at the alignment used in the balance calibration. The position-sensing elements of the main control system are not considered sufficiently accurate, and therefore a separate but similar optical system is used. MIT[61] uses two overlapping photocells and subtracts their outputs; the net output has a sharp maximum when the light beam passes the overlap, allowing repeatable positioning within about 0.001 in. The over-all error is 1% when the calibration is performed just prior to the run but may exceed 5% if the calibration is made on a different day.

Pressure measurements must necessarily be made by unconventional means. Slender probes downstream of the model have been used to measure base pressures, but these again raise the question of possible flow-field distortion caused by the probe. ONERA[58] has successfully used an optical manometer technique for base pressure measurement, a model-mounted membrane deflects in proportion to the Δp between the measured and reference pressures. (Reference pressures are obtained separately using a sting support.) Two membrane-mounted mirrors reflect incident light paths separated an initial distance d_0. Two mirrors are used to make the pressure measurement independent of most model motions. The calibration data[58] show excellent linearity for $\Delta p \sim (d\text{-}d_0)$. The over-all accuracy is quoted as $\pm 2.3\%$ at $M_\infty = 7.6$ and $Re = 2 \times 10^5$. Better accuracy should be obtained at higher base pressures and with more sensitive membranes.

Telemetry techniques have also been attempted.[62, 63] The suspension system magnetic fields did not affect either the level or frequency of the signal. In a system that used FM equipment developed for hypervelocity range use,[63] results showed errors of less than 3% at the beginning of each run, but these errors increased as the run progressed because of interaction between telemetry frequency and temperature.

The magnetic suspension technique offers promise for dynamic stability measurements. In principle, elastic restraint is available for all degrees of freedom and could be made adjustable for the various test condition requirements. Either free- or forced-oscillation methods may be used. Laboratories active in magnetic model support are also working on the dynamic stability application. The control and readout systems will, of course, be even more complex than the ones now in use for control and aerodynamic measurements.

In conclusion, the magnetic model suspension concept in its present state of development is not without its shortcomings: it involves complex and expensive equipment; a control system malfunction could result in complete loss of the model; it is temperature sensitive, particularly to the temperature of the magnetic model core; calibrations are lengthy, because of the interactions and the need for checking at all model angles, and should be done daily; and pressure measurements are neither accurate nor convenient to obtain, and the number of pressures which can be measured is limited. Perhaps it is not surprising that the magnetic methods have not received wider acceptance. However, magnetic model suspension does satisfy the requirements for certain wind-tunnel investigations where support system interference is critical, such as some in the transonic range and many low-density experiments.

Large-Model Tests at Supersonic Speeds

Model Limitations for Starting

For a given model and M_∞, the maximum allowable model cross-sectional area is dictated by the limiting area (model blockage) which will still permit starting of the flow. The model length is limited by the reflection of the bow wave with proper allowance for the angle-of-attack range and with some margin to minimize the possible effect of the reflected disturbance on the subsonic wake. The limiting model area is very commonly defined as

$$A_M/A = 1 - (P_{0_1}/P_{0_2})(A^*/A) \tag{6}$$

where A_M/A is the ratio of the maximum cross-sectional area of the model to that of the tunnel, P_{0_1}/P_{0_2} is the ratio of the total pressures ahead of and behind a normal shock wave at the M_∞ being established, and A^*/A is the ratio of the sonic to tunnel cross-sectional area for isentropic flow to M_∞; that is, A is the geometric area of the tunnel less an allowance for the displacement thickness of its boundary layer. Equation (6) represents a one-dimensional theory based on the physical premise that the starting process in a supersonic wind tunnel does involve the passage of a normal shock wave through the nozzle and test region with choking at the minimum area section.

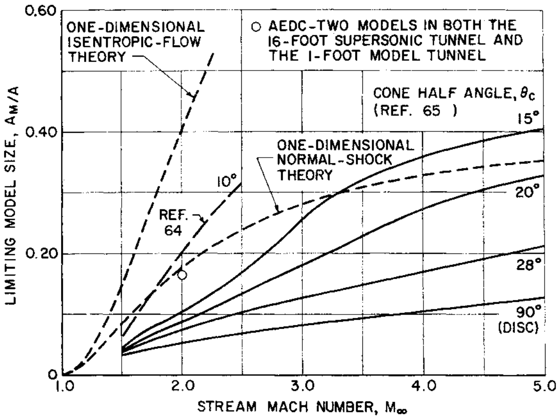

Fig. 21 Limiting model blockage for cones.

The actual starting process is a very complex one which cannot be approximated satisfactorily by the entropy increase across a normal shock wave. Draper[64] and Schueler[65] have shown the great dependence of maximum model blockage for starting upon the degree of bluntness. The results for cones with various half-angles are summarized in Fig. 21 and are compared with the normal shock theory, Eq. (5), and with the limit represented by the isentropic flow theory [Eq. (6) with $P_{0_1}/P_{0_2} = 1$]. Obviously, the normal shock limit can be exceeded with the more slender cones. Draper[64] has analyzed the starting mechanism for slender cones, showing that the starting shock-wave structure just downstream of the cone tip consists of the cone oblique wave near the cone surface and a bifurcated wave near the tunnel wall. Both mechanisms provide relief from normal shock losses; this relief increases with M_∞.

Also spotted on Fig. 21 is a point representing two large induction system models of the same maximum area but of irregular cross-sectional area (very crudely as ogive-cylinder combinations). The equivalent cone half-angles at the front of the models are in the 10°–15° range. Thus, there is some indication that large models of irregular shape have reasonably predictable starting limits which depend on nose bluntness.

Another problem is the effect of model blockage on the pressure ratios required to start and operate the wind tunnel. In Fig. 22, a comparison is made between one of the large induction system models and a small sting-mounted model in the AEDC 16-ft supersonic tunnel. The blockage for the large model was 16.5%, whereas the largest item in the small model case was the 4.8% blockage due to the sting support strut. It is apparent that model size had little effect on either the starting or operating pressure ratios; in fact, the starting values were even slightly lower for the large model. Although this result may seem somewhat surprising at first, one can consider a large, long, slender model as effectively an extension of the tunnel converging-diverging diffuser,

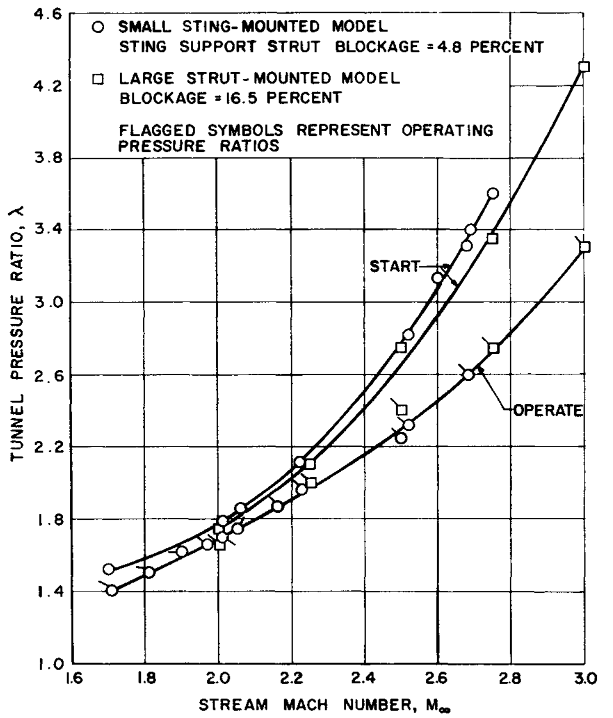

Fig. 22 Comparison of minimum starting and operating pressure ratios in the AEDC 16-ft supersonic tunnel.

and it is well known that increased diffuser length usually improves both the starting and flow-breakdown pressure ratios.

The previous discussion assumed that the tunnel would be operated at the Mach number at which it was started. However, an appreciable increase in model size over the limiting values of Fig. 22 can be achieved if the tunnel is equipped with a nozzle that can be varied while the air is flowing. One simply establishes the flow at a higher M_∞ than finally desired, with its correspondingly greater allowable area ratio, and then reduces M_∞ to the desired value. The limit of this process depends on the over-all entropy increase due to blockage, which is smaller after flow is established than during starting and often is much less than normal shock value, so that model sizes considerably in excess of those given by Eq. (6) are possible. Dayman[66] has presented results for the reduction in Mach number possible after start at Mach numbers of 1.3 to 2.2 for cone-cylinder models having cone-half-angles of 15° and 20°. The correlation of these data showed a linearly increasing increment of area ratio with M_∞.

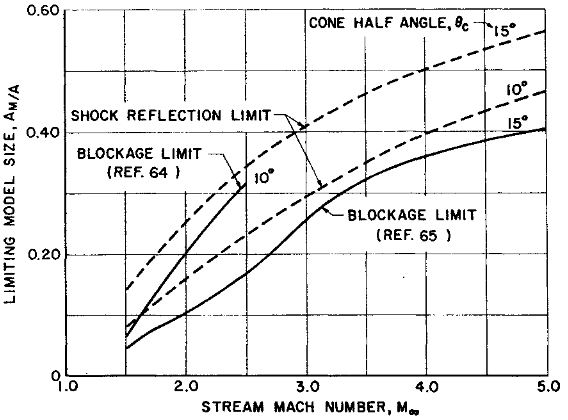

Fig. 23 Comparison of blockage and shock reflection limits for slender cones in a square tunnel.

Wall Interference

Slender bodies will be subject to the limitation due to the bow-shock-wave reflection from the tunnel walls before the blockage limit for starting is reached. The limiting case of the cone base area and M_∞ which correspond to the intersection of the bow-shock reflection with the edge of the cone base for a square tunnel and zero cone angle-of-attack is shown in Fig. 23. The comparison of the shock reflection and blockage limits for cone half-angles of 10° and 15° clearly shows that the blockage limit cannot be attained without impingement of the reflected shock on the 10° cone, except possibly at the very lowest Mach numbers. At 15° it is still possible to avoid reflected-shock impingement. However, in any practical slender body case where angle of attack is required, where an afterbody is used, and/or where base flow interference effects must be considered, the limiting model size will be dictated by shock reflection up to considerably higher equivalent nose cone angles than the values of Fig. 23. Hence, if testing of long models with complete simulation of the external aerodynamics is required, a means of reducing wall interference effects is needed. One method is to employ the same wave cancellation techniques which were used in the development of perforated wind-tunnel walls for transonic speeds.[67, 68]

A sample result for the perforated-wall technique[69] is reproduced as Fig. 24. The significant feature is the attenuation of both the reflected-bow and shoulder-expansion waves, resulting in reasonable agreement with the calculated interference-free pressure distribution. These results were considered sufficiently encouraging to warrant construction of a set of perforated walls for the 16-ft tunnel. The design chosen consists of holes slanted 60° from perpendicular and a plate-thickness/hole-diameter ratio of 1.0. The open-area ratio of 10% is defined in terms of hole diameter. The slanted holes were chosen for their superior expansion wave cancellation properties. The design M_∞ is 2.0; Pindzola and Chew[68] have shown that the required wall characteristics vary only very slowly for $M_\infty \geq 2.0$.

Another advantage of perforated walls is that, since mass removal through the walls is an integral part of the system, much of the mass removed during the starting process represents the model displacement, i.e., the very strong shock waves encountered with blocked flow[66] will not be supported as readily by perforated walls. Hence, an increase in allowable blockage area may result. The limit of this probable increase would depend on the capacity of the suction system or the mass flow limits of the walls due to choking, whichever occurs first. There is also a chance that improved diffuser efficiency will result from the removal of much of the boundary layer. However, these factors still require much experimental verification. The price for perforated walls is the need for a plenum chamber around the test section and a suction system of mass flow capacity, relative to the test sec-

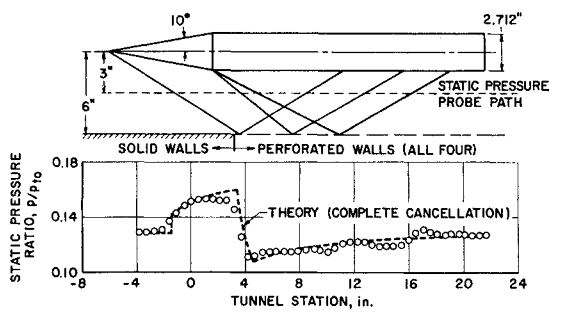

Fig. 24 Static pressure distribution 3 in. below the tunnel centerline with a 4% blockage, 10° (half-angle) cone-cylinder model at Mach 2.0; divergence angle of each of two walls is 1.0°.

tion flow, roughly equal to the maximum blockage ratio at which reasonable flow is desired over the entire model length.

The Image Model Technique

For certain types of bodies, such as re-entry nose cones, aerodynamic data are required for a large angle-of-attack range, often from 0° to 180°. Obtaining such data by the conventional support-sting methods requires at best a very complex model, balance, and sting combination (or several different models and stings), and a number of time-consuming model changes. One method that insures that the full-angle range can be readily obtained is that of a half-model mounted on a reflection plane (Fig. 25). J. D. Gray and J. H. Jones at AEDC (ARO, Inc., Von Karman Gas Dynamics Facility) have suggested another technique, which they call the image-model method. Figure 26 shows that this technique simply involves splitting the model along the pitch plane of symmetry and measuring the forces on only the outboard half. The inboard portion is attached to a strut and pitch mechanism which has full-angle range capability.

Gray and Jones obtained a direct comparison of the three-component aerodynamic data for the model of Fig. 25 using the reflection plane, image-model, and conventional sting-mounted techniques at $M_\infty = 3$ (Fig. 27). The reflection-plane data show deviations from the sting-mounted results in the vicinity of 60° for all components and 180° for axial force. These deviations are attributed to the normal shock waves generated by the extreme bluntness which this particular model presents to the approaching airstream at $\alpha \approx 57°$ and 180°. At $M_\infty = 3$, these waves are sufficiently strong to trigger separation of a turbulent boundary layer on the reflection plane. At 180°, the separation effect shows up only in axial force because of the small magnitude of normal force and pitching moment due to model symmetry. In contrast, the image-model data show good agreement with the sting-mounted results. The small discrepancies evident near 57° are believed to be associated with air leakage through the gap, since some preliminary data obtained without the gap windshield showed appreciably greater deviations from the sting-mounted case. Thus, there is the possibility of obtaining very high quality data with improved gap seal designs.

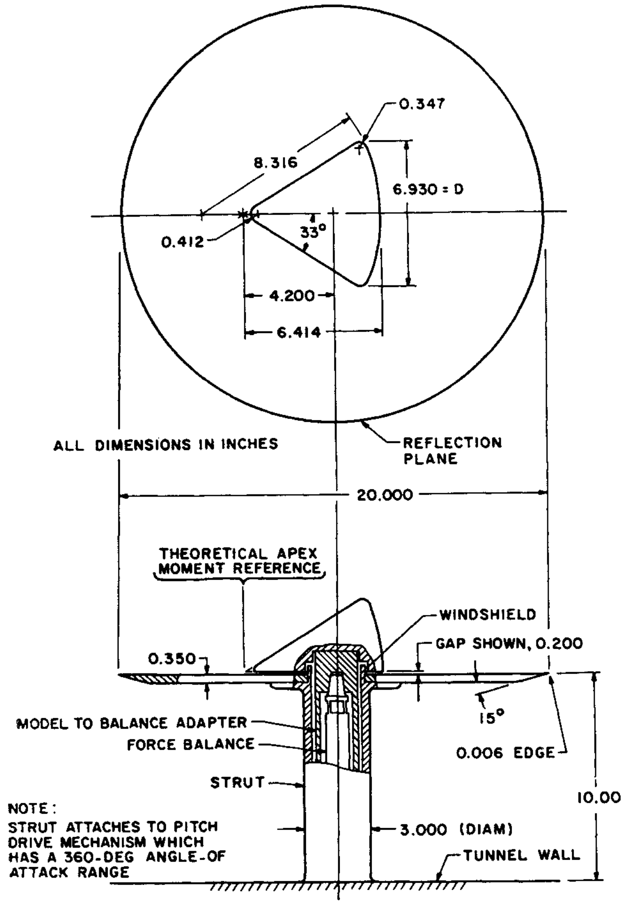

Fig. 25 Reflection plane installation.

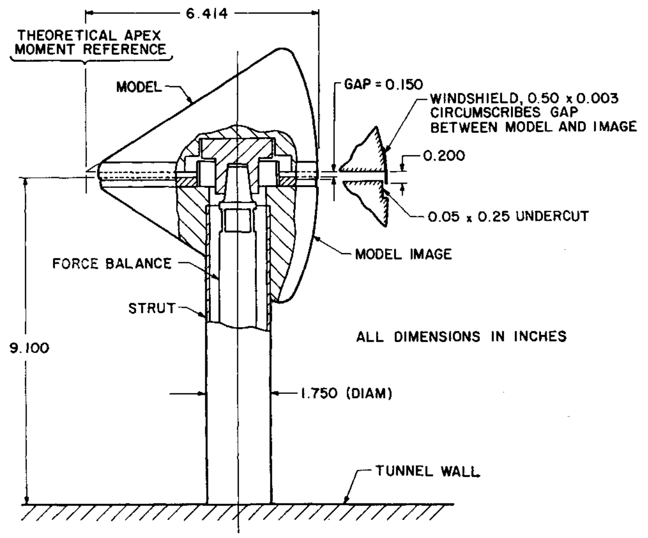

Fig. 26 Image-model installation.

The image-model technique offers promise beyond that of the convenience of testing models for very large α ranges. This promise is the possibility of eliminating the sting support strut for that large class of experiments where sting interference is a problem. Care must be taken with both the gap seal and the design of the attachment from the tunnel wall to the image portion of the model. In the latter case, a major problem would be to avoid interference of this model-wall attachment on the half of the model attached

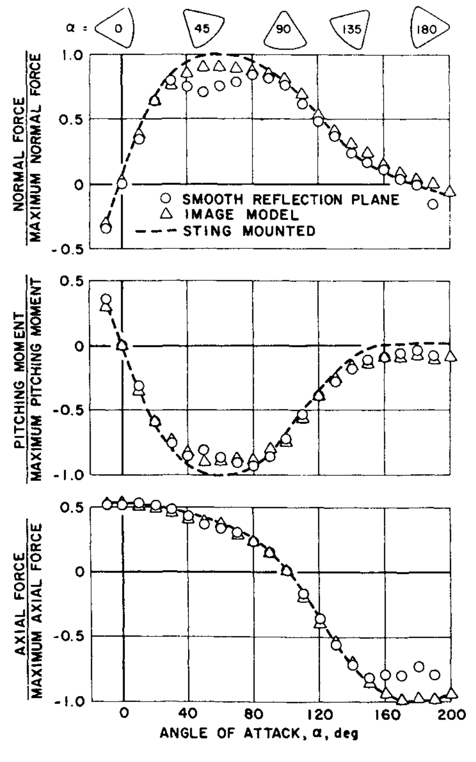

Fig. 27 Comparison of data for three methods of model support.

to the balance. The transonic Mach number range obviously will be quite critical.

References

[1] Pindzola, M., "Jet simulation in ground test facilities," AGARDograph 79 (1964).

[2] Bressette, W. E., "Some experiments relating to the problem of simulation of hot jet engines in studies of jet effects on adjacent surfaces at a free-stream Mach number of 1.80," NACA RM L56E07 (July 1956).

[3] Lee, G., "An investigation of transonic flow fields surrounding hot and cold sonic jets," NASA TN D-853 (April 1961).

[4] Love, E. S., Grigsby, C. E., Lee, L. P., and Woodling, M. J., "Experimental and theoretical studies of axisymmetric free jets," NASA TR R-6 (1959); supersedes NACA RM L54L31, NACA RM L55J14, NACA RM L56G18, and NACA TN 4195.

[5] Goethert, B. H. and Barnes, L. T., "Some studies of the flow pattern at the base of missiles with rocket exhaust jets," Arnold Engineering Development Center TR-58-12 (June 1960); originally published in October 1958 and reissued as unclassified and nonproprietary.

[6] Kawamura, R., "Reflection of a wave at an interface of supersonic flows and wave patterns in a supersonic compound jet," J. Phys. Soc. Japan **7** (September-October 1952).

[7] Pindzola, M. and Hensel, R. W., "High altitude jet spreading and some associated interference problems on space vehicles," Proceedings of the Fluid Dynamic Aspects of Space Flight, AGARD Fluid Dynamics Panel, Marseille, France (April 1964), to be published as AGARDograph 87.

[8] Tempelmeyer, K. E., "An analytical study of hot jet simulation with a cold gas mixture," Arnold Engineering Development Center TN-58-54 (September 1958).

[9] Runckel, J. F. and Swihart, J. M., "A hydrogen peroxide hot-jet simulator for wind-tunnel tests of turbojet-exit models," NASA Memo 1-10-59L (February 1959).

[10] Evans, A. J., "The simulation of the effects of internal flow in wind tunnel model tests of turbojet powered aircraft," Seventh Meeting of the Wind Tunnel and Model Testing Panel, Ottawa, Canada, AGARD (AG19/P9) (June 1955).

[11] Herstine, G. L., Burge, G. W., and Marion, E. D., "Base heating experimental programs for Saturn S-IV Stage," Fairchild Fund Paper FF-31, presented at the IAS 30th Annual Meeting, New York (January 1962).

[12] Hensel, R. W., "Rocket testing in the AEDC propulsion wind tunnel," Arnold Engineering Development Center TN-60-136 (July 1960).

[13] Gerke, P. D., "Characteristics of rocket engine plumes in supersonic flow," Arnold Engineering Development Center TDR-62-98 (July 1962).

[14] Goethert, B. H., "Base flow characteristics of missiles with cluster-rocket exhausts," Aerospace Eng. (March 1961); also IAS Paper 60-89 (June 1960).

[15] Page, R. H. and Dixon, R. J., "Base heating on a multiple propulsion nozzle missile," AIAA Paper 63-179 (June 1963).

[16] Peters, C. E., "Annular nozzles for missile base flow testing," Arnold Engineering Development Center TN-60-62 (May 1960).

[17] Peters, C. E. and Wehofer, S., "A general investigation of two-stream supersonic diffusers," Arnold Engineering Development Center TDR-62-22 (March 1962).

[18] Westkaemper, J. C., "An analysis of slug-type calorimeters for measuring heat transfer from exhaust gases," Arnold Engineering Development Center TN-60-202 (November 1960).

[19] Wehofer, S., "Rocket heat transfer measuring devices and techniques," Arnold Engineering Development Center TDR-63-93 (July 1963).

[20] Weatherston, R. C. and Hertzberg, A., "Investigation of rocket flow problems by means of short duration flow devices," ARS J. **31,** 1149–1151 (August 1961).

[21] Bird, K. D., Reece, J. W., and Smith, W. E., "The application of short duration techniques to the experimental study of base heating," Cornell Aeronautical Lab. Rept. 115, 2nd Symposium of Rocket Testing in Simulated Space and High Altitude Environments at the Arnold Engineering Development Center (June 1961).

[22] Bird, K. D., Matthis, C. L., and Reece, J. W., "The application of short duration techniques to the experimental study of base heating, Part I: High-altitude testing technique and experimental results for a 4-engine rocket configuration," Cornell Aeronautical Lab. Rept. HM-1510-Y-1(I) (April 1962).

[23] Vidal, R. J. "Fast response temperature measuring instrumentation," ARS Preprint 327-56 (September 1956); also "Transient surface temperature measurements," Cornell Aeronautical Lab. Rept. 114 (March 1962).

[24] Martin, J. F., Duryea, G. R., and Stevenson, L. M., "Instrumentation for force and pressure measurements in a hypersonic shock tunnel," Cornell Aeronautical Lab. Rept. 113, Second National Symposium on Hypervelocity Techniques, Denver, Colo. (March 1962).

[25] Matthis, C., Muench, R., and Rickard, W., "The design and development of a short-duration constant pressure combuster for use in rocket base heating investigations," Cornell Aeronautical Lab. Rept. HM-1510-Y-2 (December 1962).

[26] Ihrig, H. K., Jr. and Korst, H. H., "Quasi-steady aspects of the adjustment of separation flow regions to transient external flows," AIAA J. **1,** 934–937 (April 1963).

[27] Rickard, W. D. and Dennis, R. J., "High altitude base heating and pressure distribution investigations on the Saturn S-IV 6-engine stage rocket using short duration technique," Cornell Aeronautical Lab. Rept. HM-1510-Y-3 (June 1963).

[28] Beheim, M. A. and Obery, L. J., "Wind tunnel studies of booster base heating," Astronaut. Aerospace Eng. **1,** 111–117 (February 1963).

[29] Rainey, A. G. and Runyan, H. L., "Structural dynamics aspects of the manned lunar space vehicle launch phase," Society of Automotive Engineers Preprint 513C (April 1962).

[30] Austin, R. F. and Prunty, C. C., "Characteristics of unsteady pressures on 0.24 and 0.06-scale models of the Mark 4 re-entry body at transonic speeds," Arnold Engineering Development Center TDR-62-71 (April 1962).

[31] Chevalier, H. L. and Robertson, J. E., "Unsteady pressures and scale effects on models of the Titan B Mark 4 re-entry body at transonic speeds," Arnold Engineering Development Center TDR-62-178 (November 1962).

[32] Jones, G. W., Jr. and Faughner, J. T. Jr., "Investigation of buffet pressures on models of large manned launch vehicle configurations," NASA TN D-1633 (May 1963).

[33] Davis, E. L., Jr., "The measurement of unsteady pressures in wind tunnels," AGARD Rept. 169, NATO, Paris (March 1958).

[34] Austin, R. F. and Trail, G. C., Jr., "The design and dynamic calibration of a pressure transducer system for unsteady pressure measurements," Arnold Engineering Development Center TDR-63-29 (March 1963).

[35] Chevalier, H. L. and Todd, H. E., "Measurement of the pressure fluctuations in the test section of the 16-foot transonic circuit in the frequency range from 5 to 1000 cps," Arnold Engineering Development Center TN-61-51 (May 1961).

[36] Robertson, J. E., "Measurement of the pressure fluctuations in the test section of the 1-foot transonic tunnel in the frequency range from 5 to 1250 cps," Arnold Engineering Development Center TDR-62-109 (May 1962).

[37] Chevalier, H. L. and Robertson, J. E., "Pressure fluctuations resulting from an alternating flow separation and attachment at transonic speeds," Arnold Engineering Development Center TDR-63-204 (November 1963).

[38] Robertson, J. E. and Chevalier, H. L., "Characteristics of steady-state pressures on the cylindrical portion of cone-cylinder bodies at transonic speeds," Arnold Engineering Development Center TDR-63-104 (August 1963).

[39] Liepmann, H. W., "Parameters for use in buffeting flight tests," Douglas Aircraft Co. Rept. SM-14631 (January 1953).

[40] Cole, H. A., Jr., "Dynamic response of hammerhead launch vehicles to transonic buffeting," NASA TN D-1982 (October 1963).

[41] Palmer, W. E., "A wind-tunnel investigation of the low-amplitude damping in yaw and directional stability of a fuselage-tail configuration at Mach numbers up to 1.10," NACA RM-L57C15 (1957).

[42] DuBose, H. C., "Static and dynamic stability of blunt bodies," AGARD Rept. 347, NATO, Paris (April 1961).

[43] Beam, B. H., "A wind-tunnel test technique for measuring the dynamic rotary stability derivatives including the cross derivatives at high Mach numbers," NACA Rept. 1258 (1956); supersedes NACA TN 3347 (January 1955).

[44] Braslow, A. L., Wiley, H. G., and Lee, C. Q., "A rigidly forced oscillation system for measuring dynamic stability parameters in transonic and supersonic wind tunnels," NASA

TN D-1231 (March 1962); supersedes NACA RM L58A28 (1958).

[45] Brilat, R. P. and Wiley, H. G., "Dynamic longitudinal and directional stability derivatives for a 45° sweptback-wing airplane model at transonic speeds," NASA TM X-39 (August 1959).

[46] Welsh, C. J., Hance, Q. P., and Ward, L. K., "A forced-oscillation balance system for the von Karman facility 40- by-40-inch supersonic tunnel," Arnold Engineering Development Center TN-61-63 (May 1961).

[47] Riddle, C. D., "A description of a forced-oscillation balance," Arnold Engineering Development Center TDR-62-68 (May 1962).

[48] McKee, M. L., "A description of the control and readout system for a forced-oscillation balance," Arnold Engineering Development Center TDR-62-69 (June 1962).

[49] Welsh, C. J., Ledford, R. L., Ward, L. K., and Rhudy, J. P., "Dynamic stability tests in hypersonic tunnels and at large model amplitudes," Arnold Engineering Development Center TR-59-24 (December 1959).

[50] Shantz, I. and Groves, R. T., "Dynamic and static stability measurements of the basic finner at supersonic speeds," U. S. Naval Ordnance Lab. NAVORD Rept. 4516 (January 1960).

[51] Hodapp, A. E., Jr. "Evaluation of a gas bearing pivot for a high amplitude dynamic stability balance," Arnold Engineering Development Center TDR-62-221 (December 1962).

[52] Dayman, B., Jr., Brayshaw, J. M., Jr., Nelson, D. A., Jaffe, P., and Babineaux, T. L., "The influence of shape on aerodynamic damping of oscillatory motion during Mars atmosphere entry and measurement of pitch damping at large oscillation amplitudes," Jet Propulsion Lab. Technical Rept. 32-380 (February 1963).

[53] Dayman, B., Jr., "Simplified free-flight testing in a conventional wind tunnel," Jet Propulsion Lab. Technical Rept. 32-346 (October 1962).

[54] Holmes, F. T. "Axial magnetic suspensions," Rev. Sci. Instr. **8**, 444–447 (November 1937); also Phys. Rev. **51**, 689 (1937).

[55] Tournier, M., Dieulesaint, E., and Laurenceau, P., "Étude realisation, et mise au point d'une suspension de maquette aerodynamique par action magnetique pour une petite soufflerie" ("Design, construction, and adjustment of a magnetic suspension system for aerodynamic models in a small wind tunnel"), Office Nationale d'Études et de Recherches Aeronautiques, Paris, N.T.1/1579AP.

[56] Tournier, M. and Laurenceau, P., "Perfectionnements a la suspension magnetique des maquettes" ("Improvement in the magnetic suspension of models"), Office Nationale d'Études et de Recherches Aeronautiques, Paris, N.T. 5/1579 AP (December 1956).

[57] Laurenceau, P. and Desmet, E. "Adaptation de la suspension magnetique des maquettes aux souffleries S. 19 et S.8" ("Adaptation of magnetic suspension of models to wind tunnels S.19 and S.8") Office Nationale d'Études et de Recherches Aeronautiques, Paris, N.T. 7/1579 AP (January 1957).

[58] Dubois, G. and Rouge, C. "On a method for measuring the base pressure," Rech. Aeron. **79** (November-December 1960); translated by Univ. of Va., Rept. AST-4443-102-61U (May 1961); also Air Force Office of Scientific Research 1020 and Armed Services Technical Information Agency AD-260634.

[59] Parker, H. M., May, J. E., and Nurre, G. S., "An electromagnetic suspension system for the measurement of aerodynamic characteristics," Univ. of Va. Rept. AST-443-106-62U, Contract AF 49(638)-1022 (March 1962); also Air Force Office of Scientific Research 2294.

[60] Tilton, E. L., III, Parkin, W. J., Covert, E. E., Coffin, J. B., and Chrisinger, J. E., "The design and initial operation of a magnetic model suspension and force measurement system," Aeronautical Research Labs. (USAF-OAR) Rept. ARL 63-16, Contract AF 33(616)-7023, Wright-Patterson Air Force Base, Ohio (January 1963).

[61] Covert, E. E. and Tilton, E. L., III., "Calibration of a magnetic balance system for drag, lift, and pitching moment," Massachusetts Institute of Technology Aerophysics Lab. (May 1963).

[62] Beaussier, J., "Telemesure pour maquette suspendue magnetiquement en soufflerie" ("Telemetering for a magnetically suspended model in a wind tunnel"), Rech. Aeron. **82** (May–June 1961).

[63] Clemens, P. L., "Radio telemetry of stagnation pressure from a wind tunnel model magnetically supported in supersonic flow," Arnold Engineering Development Center TDR-62-141 (July 1962).

[64] Draper, A. C., "Redefinition of the limiting concept for supersonic wind tunnel blockage," Wright Air Development Center TN-58-186, Armed Service Technical Information Agency AD 155692 (June 1958).

[65] Schueler, C. J., "An investigation of the model blockage for wind tunnels at Mach numbers 1.5 to 19.5," Arnold Engineering Development Center TN-59-165 (February 1960).

[66] Dayman, B., Jr., "Prediction of blocking in the supersonic wind tunnel during an attempted start," Jet Propulsion Lab. Rept. 20-109 (June 1957).

[67] Goethert, B. H., *Transonic Wind Tunnel Testing* (Pergamon Press, Inc., New York, 1961), AGARDograph 49.

[68] Pindzola, M. and Chew, W. L., "A summary of perforated wall wind tunnel studies at the Arnold Engineering Development Center," Arnold Engineering Development Center TR-60-9 (August 1960).

[69] Ramm, H. and Jones, M., "Use of perforated walls for shock cancellation at supersonic speeds," Arnold Engineering Development Center TR-59-15 (August 1959).